Chemical Science

ROYAL SOCIETY OF CHEMISTRY

EDGE ARTICLE

View Article Online
View Journal | View Issue

Cite this: *Chem. Sci.*, 2021, **12**, 15928

All publication charges for this article have been paid for by the Royal Society of Chemistry

An unexpected non-conjugated AIEgen with a discrete dimer for pure intermolecular through-space charge transfer emission†

Xiujie Jiang,‡[a] Wei Tao,‡[a] Cheng Chen,[a] Guoyong Xu,[a] Haoke Zhang *[bcd] and Peifa Wei *[ad]

Received 3rd October 2021
Accepted 21st November 2021

DOI: 10.1039/d1sc05426k

rsc.li/chemical-science

Manipulation of the charge transfer in donor–acceptor-type molecules is essential for the design of controllable aggregate luminescent materials. Apart from the traditional through-bond charge transfer (TBCT) systems which suffer from complicated structural design, poor tunability and low quantum efficiency, through-space charge transfer (TSCT) has been proved as an alternative yet facile strategy in tuning photophysical processes. In this work, by simply changing nucleophilic reaction bases, a traditional conjugated acrylonitrile **AP1** and an unexpected non-conjugated **AP2** with a carboxamide-functionalized oxirane linker could be obtained. The long-range π–π stacking in conjugated **AP1** results in mixed intramolecular TBCT plus intermolecular TSCT emission. However, facilitated by the steric hindrance effect of the big oxirane connector and the unique discrete dimer packing, non-conjugated **AP2** exhibits pure and efficient intermolecular TSCT emission in both aggregate and crystalline states. The flexibility of the non-conjugated character further leads to better reversible stimuli-responsiveness to mechanical force for **AP2** than for the rigid **AP1**.

Introduction

Organic photoluminescent materials are widely used in numerous fields such as optoelectronic devices,[1] bioimaging,[2] medical diagnosis,[3] chemical sensing,[4] *etc.* due to their favorable flexibility, biocompatibility, processability and structural diversity. Compared with a molecule in a molecularly dispersed state, its aggregate state exhibits macroscopic optical properties and functions that are completely different from those of a single molecule owing to a variety of intermolecular interactions. For example, aggregation-caused quenching (ACQ) is a typical representative,[5] which is characterized by high luminescence in solution, but weak or no emission in the aggregate state. This is unfavorable for the study of the luminescence mechanism and the regulation of luminescence behavior in the aggregate state. The aggregation-induced emission (AIE) phenomenon proposed by Tang is completely the opposite: fluorescent molecules do not emit light in dilute solution but exhibit significant fluorescence enhancement in the aggregate state.[6,7] This brings the research on photoluminescent materials from molecular science to aggregate science.[8–11]

From the perspective of aggregate science, how to achieve high-efficiency and controllable luminescence in aggregates through structural design is of great significance for the understanding of the luminescence mechanism and the extension of luminescence systems. Constructing charge transfer (CT) systems is a common and effective method to control the emission wavelength and efficiency.[12–14] So far, most of the luminescence systems with CT characteristics have been based on through-bond charge transfer (TBCT) emission.[15–17] The organic fluorophores mainly connect the electron donors (D) and electron acceptors (A) through double bonds, triple bonds, heteroatoms, or aromatic rings to form structures with larger π conjugation, which enables strong electron coupling between the donor and acceptor through covalent bonds.[18,19] However, the strong TBCT effect in the conjugate system often leads to redshift emission accompanied by a significant decrease in quantum efficiency, which is unfavorable for practical applications.[20,21] Therefore, the development of new methods to balance the CT intensity is essential for the design of controllable aggregate luminescent materials.

[a]*Institutes of Physical Science and Information Technology, Key Laboratory of Structure and Functional Regulation of Hybrid Materials of Ministry of Education, Anhui Graphene Engineering Laboratory, Anhui University, Hefei, China. E-mail: pfwei@ahu.edu.cn*

[b]*MOE Key Laboratory of Macromolecular Synthesis and Functionalization, Department of Polymer Science and Engineering, Zhejiang University, Hangzhou, China*

[c]*ZJU-Hangzhou Global Scientific and Technological Innovation Center, Hangzhou 311215, China. E-mail: zhanghaoke@zju.edu.cn*

[d]*Guangdong Provincial Key Laboratory of Luminescence from Molecular Aggregates, South China University of Technology, Guangzhou, China*

† Electronic supplementary information (ESI) available: Other experimental procedures, compound characterization, other supplementary figures and crystal data. CCDC 2090628 and 2090629. For ESI and crystallographic data in CIF or other electronic format see DOI: 10.1039/d1sc05426k

‡ These authors contributed equally to this work.

In recent years, through-space charge transfer (TSCT), which connects donors and acceptors in a spatially separate manner, has been widely adopted to effectively avoid the negative effects of strong CT.[22–27] In this motif, donors and acceptors are separated but spatially close to each other, which allows the through-space charge transfer to occur.[28–30] The currently studied TSCT system mainly relies on the intramolecular through-space interaction between the donor and acceptor.[31] However, this type of material extremely relies on a tailored structure design, especially the spatial distance of the donor and acceptor, which has a great influence on the photophysics.[32] This also brings multiple synthetic steps, which not only leads to sophisticated and tedious purification but is also time-consuming and economically unfriendly. What is worse, most of the TSCT systems still rely on large D–A conjugated π structures, which lead to high rigidity of the structures, and further bring poor solubility and difficulties in luminescence modulation.[33] Though the D–A structure connected by non-conjugated bonds can increase the molecular flexibility, it cannot regulate the intramolecular TSCT precisely, and some of them cannot even form stable intramolecular TSCT. However, in the aggregate state, the flexibility of the molecules can endow the system with enhanced intermolecular TSCT effect.[34,35] Therefore, constructing intermolecular TSCT is an effective strategy for regulating the photophysical properties of luminescent materials in aggregate states, which is easier and more controllable than the manipulation of intramolecular TSCT in the molecular state.

In this work, by simply changing the nucleophilic reaction conditions, specifically, by only tuning the base *via* the transition metal-free, nonhazardous, nontoxic, and atom-economic synthetic method, we were able to simply access conjugated acrylonitriles **AP1** and non-conjugated **AP2** based on anthracene (D) and pyridinium salt (A), as shown in Scheme 1. It is found that **AP2** exhibits unique and pure intermolecular TSCT emission in both aggregate and crystalline states based on the formation of a discrete dimer. The existence of a big carboxamide-functionalized oxirane linker in **AP2** prevents neighboring molecules from approaching the dimer, while long-range π–π stacking is observed in the conjugated **AP1**, leading to the higher emission efficiency of **AP2** than **AP1**. Besides, the synergy of flexibility of the non-conjugated linker and the comparative weak intermolecular interactions between the discrete dimer endows **AP2** with reversible stimuli-responsiveness to mechanical force, which is absent in the conjugated **AP1**.

Results and discussion

The Knoevenagel condensation is a very important transformation in organic synthesis catalyzed by bases and is widely employed for carbon–carbon bond formation, which has been used in connecting donors and acceptors to deliver conjugated AIE-active molecules.[36–39] In this work, anthracene was used as the donor while a typical pyridine salt was chosen as the acceptor. Considering that the base may have a strong effect on the efficiency of the reaction, we chose two different bases, that is, an organic base tetrabutylammonium hydroxide (TBAOH) and an inorganic base NaOH, to catalyze the reaction. However, to our great surprise, though both of the reactions proceeded in *t*-BuOH at room temperature with different bases, their reaction phenomena were quite different. The NaOH system yielded yellow precipitates which are often observed in Knoevenagel condensation reactions, indicating that we obtained a traditional π-conjugated acrylonitrile derivative, while the TBAOH system did not generate the expected precipitates but produced a clear light yellow solution instead, which was proved later to be a non-conjugated structure (Scheme 1). The difference between the two structures is the connectors between the donor and acceptor. The conjugated one was bridged by a cyanostilbene while the non-conjugated system was linked by a carboxamide-functionalized oxirane. It is noteworthy that both compounds can be obtained easily with satisfactory yields. As far as we know, it is scarcely reported that different linkages

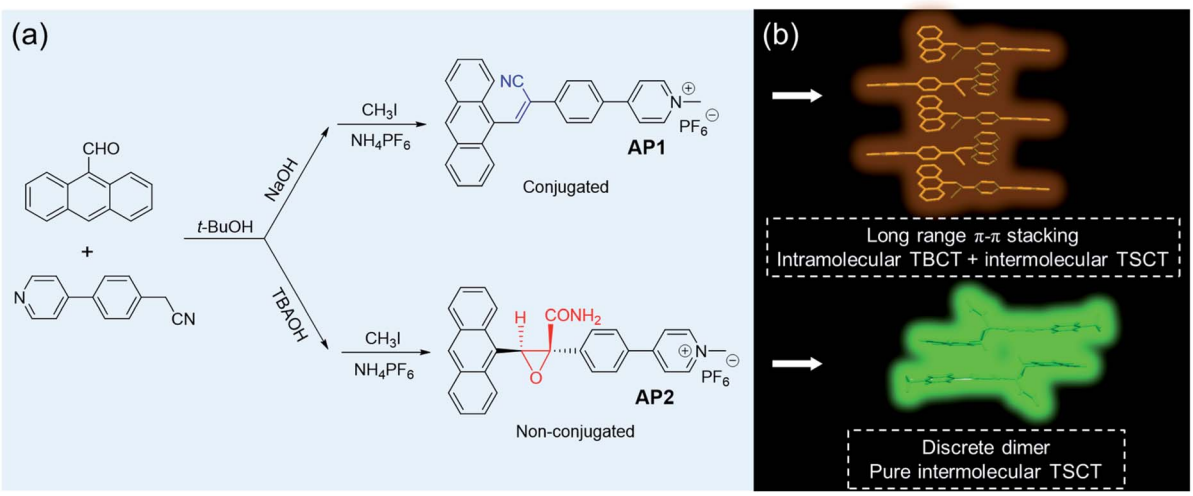

Scheme 1 (a) Synthesis of AP1 and AP2 and (b) their emission illustrations in the aggregate state.

(conjugated or non-conjugated) between donors and acceptors can be realized by simply tuning the nucleophilic reaction base. Both of the compounds were further functionalized with pyridine salts, which were named **AP1** and **AP2**, respectively. The detailed synthetic procedures, characterizations and thermal stability are summarized in the ESI (Fig. S1–S14, Schemes S1 and S2†).

It is reasonable that **AP1** can be formed by a direct nucleophilic reaction under the NaOH condition. Why was the non-conjugated **AP2** obtained under the condition of TBAOH? After dissolving π-conjugated **1** in solvents and adding TBAOH as the base, we observed that **1** could be transformed into **2** which was similar to the alkaline epoxidation of acrylonitrile as most of the references reported.[40–42] However, a key oxidant was missing in this system. The anthracene substrate would likely produce reactive oxygen species (ROS) in the presence of light which may be the oxidant.[43] This hypothesis was confirmed by repeating the reaction in the absence of light and oxygen which resulted in the expected π-conjugated acrylonitrile derivative **1** (Fig. S7†). The whole process can thus be divided into two steps: the first step involved Knoevenagel condensation to yield **1** as an intermediate; in the second step, **1** would hydrolyze to form acrylamide **3** with a *cis* configuration (Scheme S3†). The anthracene part would produce ROS in the presence of light which can further oxidize **3** to deliver the target *cis*-**2** with the amide and anthracene groups on the same face of the oxirane.

After confirming the molecular structure, we then investigated the photophysics of **AP1** and **AP2**. The color of **AP1** in CH_3CN was yellow while **AP2** was colorless, which suggests better conjugation in **AP1**. Absorption spectra of **AP1** and **AP2** were further studied in CH_3CN to confirm their electronic structures. **AP1** in the crystalline state showed one structureless broad peak located at 408 nm corresponding to the extended through-bond conjugation (TBC), while **AP2** exhibited one finely structured peak at 379 nm which almost overlapped with the maximum absorption of anthracene, suggesting the non-conjugated nature of **AP2** (Fig. 1A and S15†). The absorption maximum of anthracene was hypsochromically shifted by 10 nm from that of **AP2** and was located at 369 nm, which may be due to the hyperconjugation between the benzene ring and the methyl groups in **AP2**.[44,45] Similarly, though the molecule contains a donor and an acceptor, its CH_3CN solution only shows the characteristic fine structure emission of monomeric anthracene ranging from 370 nm to 500 nm (Fig. 1B),[46] which indicates that the two non-conjugated units of **AP2** cannot form inter- or intramolecular D–A interactions in the solution state.

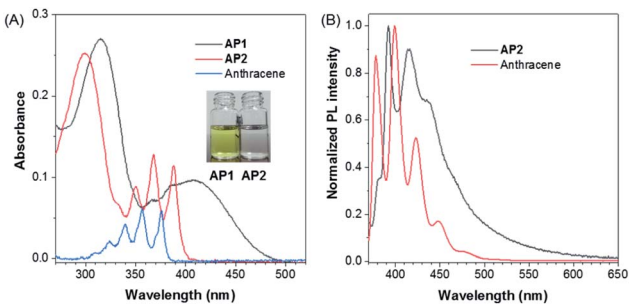

Fig. 1 (A) UV/Vis absorption spectra of **AP1**, **AP2** and anthracene in CH_3CN solution ($c = 10$ μM), respectively. Insets in (A): photos of **AP1** (left) and **AP2** (right) in CH_3CN solution under daylight. (B) Normalized emission spectra of anthracene and **AP2** in CH_3CN solution, λ_{ex} = 350 nm.

To investigate their photophysical properties in the aggregate state, the PL spectra were recorded in mixed solvents through the addition of the poor solvent hexane to the THF solution of **AP2**. It can be seen from the UV spectra that the profile of **AP2** in THF/hexane mixtures with hexane fraction (f_{Hex}) of 99% was slightly red-shifted compared to that of **AP2** in THF (Fig. 2A), suggesting the existence of weak intermolecular interaction in **AP2** aggregates. The absorption spectrum of **AP2** in the crystalline state shows an intense, broad absorption with $\lambda_{max} = 420$ nm which is redder than that of the aggregate at $f_{Hex} = 99\%$, indicating a different packing behavior in the crystalline state compared to aggregates. Considering the non-conjugated donor and acceptor character of **AP2**, it is speculated that intermolecular TSCT may lead to a broad redder absorption as the intramolecular D–A distance is too large for intramolecular TSCT. Its fluorescence spectra provide more detailed information. Fig. 2B shows that the PL spectrum in THF/hexane mixtures with low f_{Hex} exhibited a broad emission with multiple peaks at 391, 415 and 437 nm, which was assigned to anthracene emission. The intensity of the shorter-wavelength peak decreased gradually when f_{Hex} increased from 0% to 50%, which is ascribed to the polarity effect. However, a marvelous new emission band at a longer wavelength ranging from 500 to 700 nm intensified progressively with increasing the hexane fraction at $f_{Hex} \geq 60\%$, indicating the AIE nature of this longer-wavelength emission. The maximum intensity enhancement was 28-fold at $f_{Hex} = 80\%$ (Fig. 2C). The second-stage intensity annihilation of the short-wavelength at $f_{Hex} > 50\%$ should be ascribed to the energy transfer from TBC to intermolecular TSCT.

As mentioned above, the intermolecular TSCT in **AP2** aggregates was proposed as the cause of longer-wavelength emission around 560 nm. However, the polarity effects,[47,48] and intramolecular TSCT between anthracene and pyridinium salt are two more possibilities that induced the redder emission. The solvent polarity effect that may contribute to the longer-wavelength emission was first ruled out by comparing the emissions in solvents with different polarities (Fig. S16†). The emission maximum of **AP2** shows almost no change in high polarity MeOH and low polarity THF solvents. The characteristic red-shifted emission band observed in the aggregate state is not detected. To disclose the possibility of intramolecular TSCT, the PL spectrum of **AP2** in dilute THF solution ($c = 10^{-6}$ mol L^{-1}) was measured at room temperature (rt) and 77 K, respectively. As shown in Fig. S17,† from rt to 77 K, the emission intensity corresponding to the anthracene moiety is increased as non-radiative deactivation pathways are restricted, while the wavelength of the maxima emission remains unchanged and no new peak around 560 nm is observed, suggesting the negligible contribution of intramolecular TSCT to the longer-wavelength emission of **AP2**.

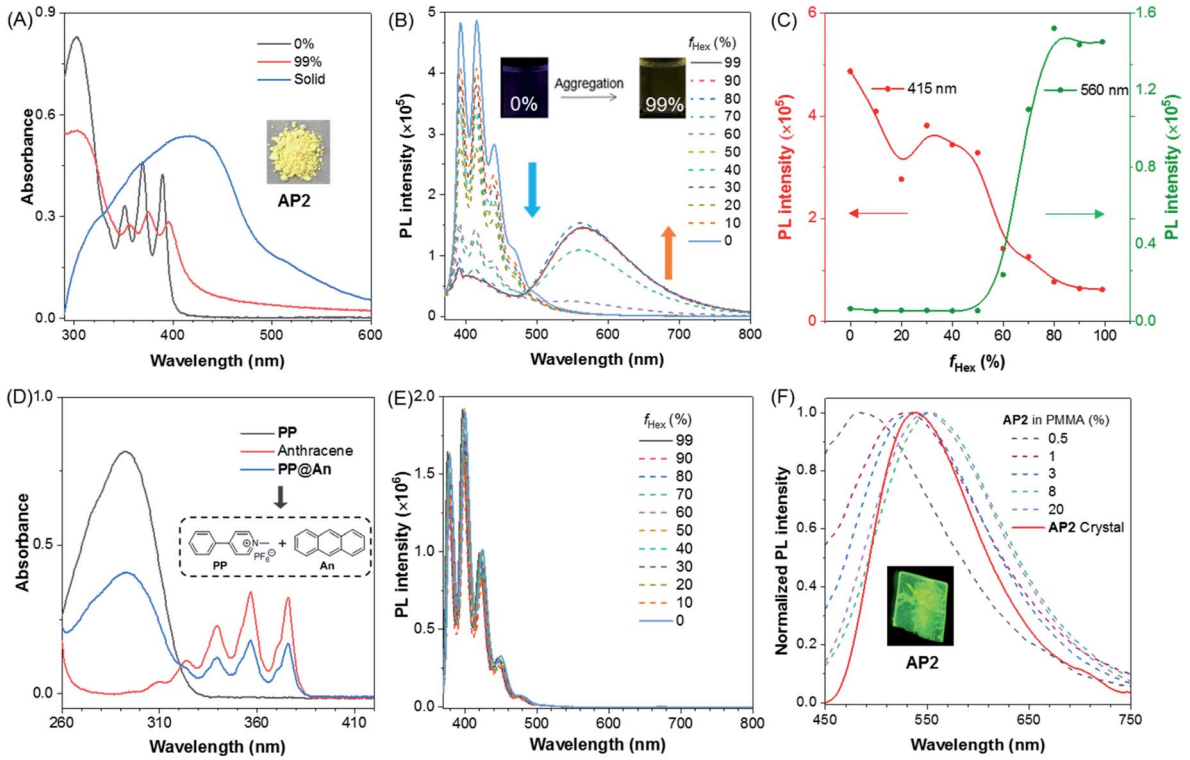

Fig. 2 (A) Absorption spectra of **AP2** in different f_{Hex} and crystalline states, $c = 10$ μM. Inset: roomlight image of **AP2** powder. (B) Emission spectra of **AP2** at different f_{Hex}, $\lambda_{ex} = 350$ nm. Inset: fluorescence photo of **AP2** at $f_{Hex} = 0\%$ and 99%, respectively. (C) Emission intensity of **AP2** at $\lambda =$ 415 nm and 560 nm with gradually increasing f_{Hex}. (D) Absorption spectra of **PP**, anthracene, and **PP@An** in CH_3CN solution, $c = 10$ μM. (E) Emission spectra of **PP@An** at different f_{Hex}, $\lambda_{ex} = 350$ nm. **An** = anthracene. (F) Emission spectra of **AP2** in the crystal state and at different concentrations (wt%) in PMMA thin film, $\lambda_{ex} = 350$ nm. Inset: fluorescence photo of **AP2** taken under a UV lamp.

To explore the role of the non-conjugated linker in generating efficient intermolecular TSCT, the donor and acceptor were physically separated instead of chemically isolating them. Then, the new compound **PP** was designed as the donor (Scheme S4†). The ^{1}H NMR spectrum of **AP2** shows that it is not a simple superposition of that of anthracene and **PP** (Fig. S18A, C and D†). In contrast, the ^{1}H NMR spectrum of the 1 : 1 molar ratio mixture of anthracene and **PP**, named **PP@An**, is exactly the superposition of the two compounds. The above results provide two conclusions: the first one is that oxirane plays a very important role in the properties of **AP2**; the second one is that simple physical mixing of anthracene and **PP** cannot produce any intermolecular interactions. In addition, the UV absorption spectra of the model compound **PP**, anthracene and **PP@An**, as well as their corresponding fluorescence emission spectra, were recorded (Fig. 2D and S19†). We found that both the absorption and fluorescence spectra of **PP@An** were simply superimposition of that of **PP** and anthracene. Neither tuning the molar ratio of **PP** and anthracene nor changing the concentration of **PP@An** from 10^{-7} to 10^{-3} mol L^{-1} could generate any new absorption or emission peaks in the solution state (Fig. S20†). Meanwhile, the PL spectra of **PP@An** in THF/hexane mixtures with different f_{Hex} were also measured but without longer-wavelength emission in the aggregate state (Fig. 2E). All these results prove the vital role of the non-conjugated oxirane linker in the generation of intermolecular TSCT for **AP2**. Physical blending of the donor and acceptor is incapable of producing efficient TSCT.

The aggregation behavior is replicated for **AP2** in five different films which were fabricated by spin-coating of the solution with **AP2** and poly(methyl methacrylate) (PMMA), the obtained films possess different doping ratios of 0.3%, 1%, 3%, 8% and 20% (**AP2**/PMMA, wt%). With the gradual addition of **AP2**, the emission wavelength of the thin film gradually redshifts from 486 nm to 550 nm (Fig. 2F), which further confirms the formation of intermolecular TSCT at high **AP2** concentration. In the crystalline state, **AP2** exhibited one comparatively sharp and green emission peak at 537 nm (Fig. 2F). The resulting long lifetime of the crystal (45.30 ns) was a possible characteristic of TSCT emission (Fig. S21† and Table

Table 1 Photophysical properties of **AP1** and **AP2**[a]

Comp.	$\lambda_{ab,soln}$ (nm)	$\lambda_{ab,crystal}$ (nm)	$\lambda_{em,crystal/ground}$ (nm)	$\Phi_{crystal}$ (%)	$\tau_{crystal}$ (ns)
AP1	408	482	623/620	1.13	2.29
AP2	379	420	537/581	18.45	45.3

[a] Abbreviation: $\lambda_{ab,soln}$ = absorption maximum in CH_3CN solution, $\lambda_{ab,crystal}$ = absorption maximum in crystalline powder, $\lambda_{em,crystal/ground}$ = emission maximum in crystal and ground powder states, $\Phi_{crystal}$ = fluorescence quantum yield of the crystal measured with an integrating sphere, $\tau_{crystal}$ = fluorescence lifetime of the crystal.

1). Variation in excitation could change only the emission intensity but not the wavelength of the luminophore (Fig. S22†), which suggests the uniform and stabilized TSCT structure in the **AP2** crystal.

The detailed structure–property relationship was revealed by single-crystal analysis. Yellow crystals were obtained by slow vapor diffusion of acetone into a *n*-pentane solution of **AP2** over a period of night at room temperature (see Table S2† for details). The anthracene and pyridine salt units are nearly spatially parallel in the crystal, and arrange into step-like offset columnar stacks of head-to-tail antiparallel dimers with close intermolecular π–π stacking (3.442 Å) and high degree of molecular overlap (Fig. 3A–F). The multiple hydrogen bonds resulting from carboxamides between the adjacent discrete dimer and column together with the nearest C–H···π (≈3.257 and 3.635 Å) of adjacent columns should be the main driving force for the formation of a 3D structure (Fig. S23 and S24†). Within each column, the slip angle of the dimer along the long molecular axis is 47.8°, while the similar slip angle of 54.6° along the short axis is also observed, resulting in a relatively large distance between the two dimers (5.445 Å). This suggests that each TSCT dimer in the crystal lattice is discrete. The crystal structure indicates that the oxirane linker and its big carboxamide substituent prevent neighboring molecules from approaching the dimer and forming the detrimental long-range π–π stacking, which results in the formation of a discrete dimer and considerable quantum efficiency (18.45%) in the crystalline state. It is noteworthy that **AP2** is racemic as *R* and *S* configurations coexist in one unit cell, suggesting the absence of stereospecificity during the reaction (Fig. S25†). The two racemic structures benefit the close arrangement of two chromophores to form the discrete dimer and thus the generation of intermolecular TSCT. Electronic excited-state delocalization of the donor and acceptor through spatial interactions results in the significantly red-shifted emission of **AP2** crystal compared to its solution.

Considering the better flexibility of non-conjugated bonds in **AP2** than the conjugated **AP1**, the TSCT emission of **AP2** is anticipated to exhibit more obvious reversible response to external stimuli. Single crystals of **AP1** were also obtained by slow vapor diffusion of i-Pr_2O into its CH_3CN solution as a comparison (see Table S1† for details). The dihedral angle between anthracene and the cyanostilbene approaches 62.88° (Fig. 3G). Different from the formation of the discrete dimer in **AP2**, infinite stacks with a small slip along both the short and long axes in **AP1** were observed in which offset head-to-tail antiparallel π-overlap of neighboring molecules by intermolecular π–π interactions (3.548 and 3.613 Å) occurred (Fig. 3K and L). The counterions in **AP1** and **AP2** play the role of a linker between two adjacent columns during the crystal packing (Fig. S26†). We can thus conclude that the reddish orange emission with much lower quantum efficiency (1.13%) in the crystalline state for **AP1** than that for **AP2** should be ascribed to the mixed intramolecular TBCT plus intermolecular TSCT effect. Considering the possibility of photoreaction of anthracene, we record the emission profiles of **AP1** and **AP2** in f_{Hex} = 99% (aggregate state) and crystalline state with different scan times (Fig. S27†). The slight or no change of profiles indicates that its influence on TSCT emission during the fluorescence study is almost negligible.

As per our expectation, the intermolecular interactions in conjugated **AP1** were stronger than those in non-conjugated

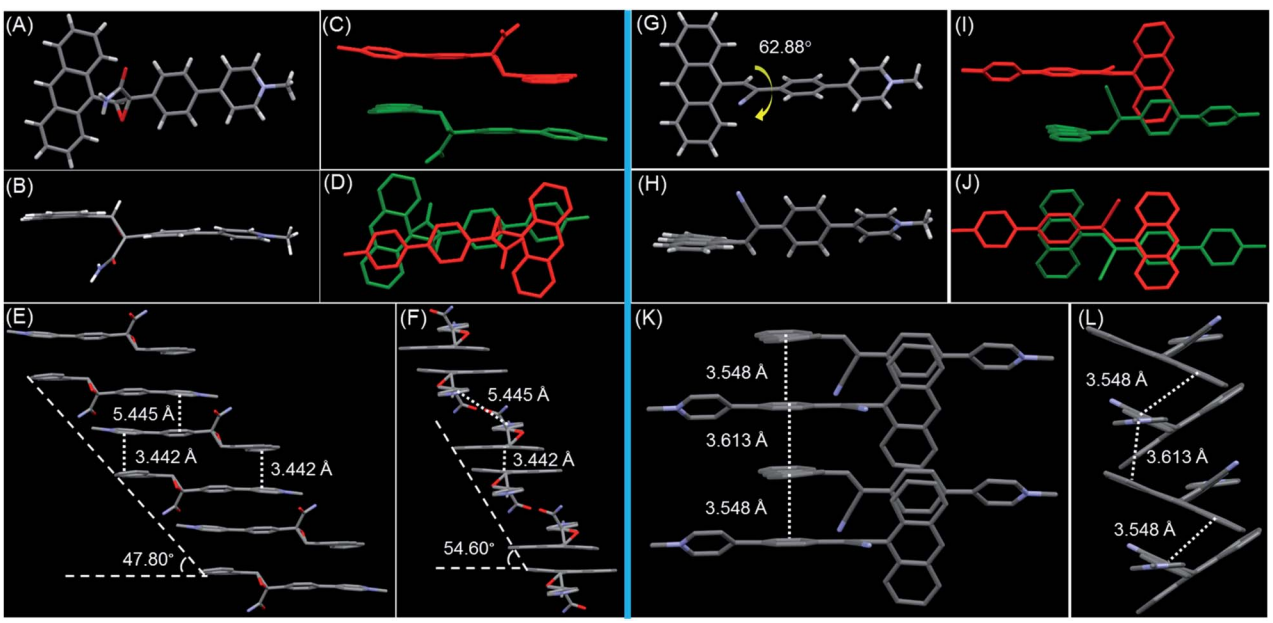

Fig. 3 **AP2** crystal analysis (left column). The molecular conformation in (A) top and (B) side view. (C) The dimer formed through TSCT viewed along the long molecule axis. (D) The overlapping in the dimer. Partial view of the molecular packing along the (E) long and (F) short molecule axes. **AP1** crystal analysis (right column). The molecular conformation in (G) top and (H) side view. The molecular overlap between adjacent molecules viewed in (I) side and (J) top view. Partial view of the molecular packing along the (K) long and (L) short molecule axes. Hydrogen atoms in (C)–(F) and (I)–(L) are omitted for the sake of clarity. The slip angles and the intermolecular distance are listed.

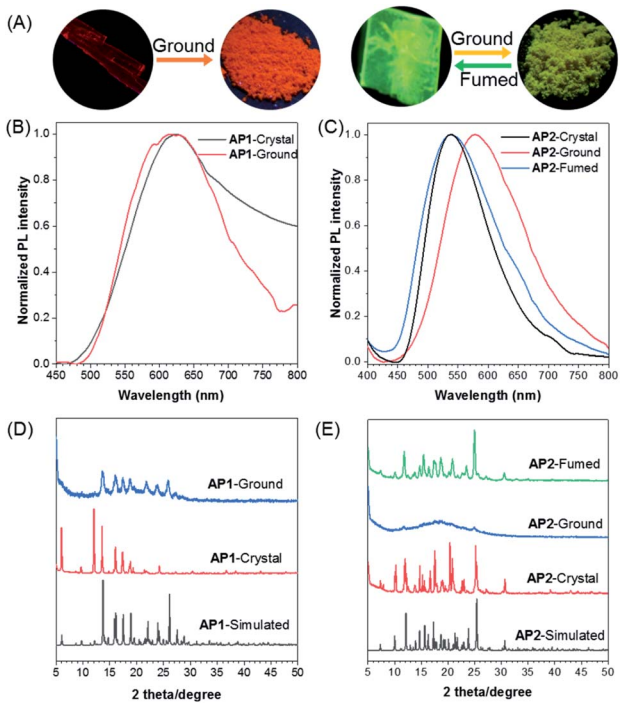

Fig. 4 (A) Fluorescence photographs of the crystal and ground powder of **AP1** (left); fluorescence photographs of the crystal, ground powder and the fumed powder of **AP2** (right). Normalized emission spectra of (B) **AP1** and (C) **AP2** crystals upon external stimuli, λ_{ex} = 360 nm. PXRD patterns of (D) **AP1** and (E) **AP2** upon external stimuli.

AP2. Their stimulus-responsive behavior under mechanical force was thus investigated. After grinding, the emission of **AP1** shows almost no change (Fig. 4A and B). The powder X-ray diffraction (PXRD) measurement confirmed that the grinding powder of **AP1** was still crystalline (Fig. 4D), indicating that the strong π–π interaction prevented the mechanical force from destroying the intermolecular forces. However, the stimulus-response behavior of **AP2** was completely different from that of **AP1**. The different emission of the original crystal and the grinding powder is large enough to be easily distinguished by the naked eye with fluorescence changes from green to yellow (Fig. 4A and C). The broad and featureless PXRD pattern for the ground samples of **AP2** reflects its amorphous characteristic (Fig. 4E). On further fumigation with acetone, both the PXRD and emission of the ground powder returned to their original state. This indicates that the synergy of flexibility of the non-conjugated linker and the comparative weak intermolecular interactions between the discrete dimer leads to better stimuli-responsiveness of **AP2**, which makes the manipulation of the aggregate structures and properties realizable.

Conclusions

In this work, we found that through simply tuning the nucleophilic reaction bases, a traditional conjugated acrylonitrile **AP1** and an unexpected non-conjugated **AP2** with carboxamide-functionalized oxirane linkage could be obtained. Interestingly, the long-range π–π stacking in conjugated **AP1** results in mixed intramolecular TBCT plus intermolecular TSCT emission, while **AP2** with discrete dimer packing could exhibit pure and efficient intermolecular TSCT emission in both aggregate and crystalline states. The physical mixing of anthracene and model compound **PP** does not work, indicating the vital role of the non-conjugated oxirane linker in producing efficient TSCT. The synergy of flexibility of the non-conjugated linker and the comparative weak intermolecular interactions between the discrete dimer led to better reversible stimuli-responsiveness to mechanical force for **AP2** than that for the rigid **AP1**. This work not only provides a simple and smart way for regulating photophysical properties in the aggregate state but also introduces an efficient method to develop stimuli-responsive luminogens.

Experimental section

Materials and methods, synthetic procedures, crystallographic data and characterizations are available in the ESI.†

Data availability

The datasets supporting this article have been uploaded as part of the ESI.†

Author contributions

X. J., W. T., H. Z. and P. W. conceived and designed the experiments. X. J. and W. T. performed the experiments. X. J., W. T., H. Z. and P. W. analyzed the data. W. T. and C. C. contributed the single crystal analysis. G. X. contributed the ^{1}H NMR experiments. X. J., H. Z. and P. W. co-wrote the paper.

Conflicts of interest

There are no conflicts of interest to declare.

Acknowledgements

This work was supported by the National Natural Science Foundation of China Grants (22001006), the Open Fund of Guangdong Provincial Key Laboratory of Luminescence from Molecular Aggregates and South China University of Technology (2019B030301003). P. W. is thankful for the support from the Innovation and Entrepreneurship Project of Overseas Returnees in Anhui Province (2020LCX017) and the Open Project of Key Laboratory of Structure and Functional Regulation of Hybrid Materials of Anhui University, Ministry of Education. H. Z. is thankful for the support from the Fundamental Research Funds for the Central Universities (2021QNA4032).

Notes and references

1 J. X. Wang, B. Y. Liang, J. B. Wei, Z. Q. Li, Y. C. Xu, T. Yang, C. L. Li and Y. Wang, *Angew. Chem., Int. Ed.*, 2021, **60**, 15335–15339.
2 E. H. K. Stelzer, *Nat. Methods*, 2015, **12**, 23–26.

3 M. R. Loizzo, R. Tundis, F. Conforti, G. A. Statti and F. Menichini, *Pharm. Biol.*, 2009, **47**, 516–520.
4 L. Chen, M. Nakamura, T. D. Schindler, D. Parker and Z. Bryant, *Nat. Nanotechnol.*, 2012, **7**, 252–256.
5 W. Watson and R. Livingston, *Nature*, 1948, **162**, 452–453.
6 J. Mei, Y. N. Hong, J. W. Y. Lam, A. J. Qin, Y. H. Tang and B. Z. Tang, *Adv. Mater.*, 2014, **26**, 5429–5479.
7 J. D. Luo, Z. L. Xie, J. W. Y. Lam, L. Cheng, H. Y. Chen, C. F. Qiu, H. S. Kwok, X. W. Zhan, Y. Q. Liu, D. B. Zhu and B. Z. Tang, *Chem. Commun.*, 2001, 1740–1741.
8 Z. Zhao, H. K. Zhang, J. W. Y. Lam and B. Z. Tang, *Angew. Chem., Int. Ed.*, 2020, **59**, 9888–9907.
9 H. K. Zhang, Z. Zhao, A. T. Turley, L. Wang, P. R. McGonigal, Y. J. Tu, Y. Y. Li, Z. Y. Wang, R. T. K. Kwok, J. W. Y. Lam and B. Z. Tang, *Adv. Mater.*, 2020, **32**, 2001457.
10 Q. Peng and Z. Shuai, *Aggregate*, 2021, **2**, e91.
11 S. Ma, S. Du, G. Pan, S. Dai, B. Xu and W. Tian, *Aggregate*, 2021, **2**, e96.
12 J.-L. Brédas, D. Beljonne, V. Coropceanu and J. Cornil, *Chem. Rev.*, 2004, **104**, 4971–5004.
13 P. Roy, A. Jha, V. B. Yasarapudi, T. Ram, B. Puttaraju, S. Patil and J. Dasgupta, *Nat. Commun.*, 2017, 1716.
14 C. J. Chen, R. J. Huang, A. S. Batsanov, P. Pander, Y. T. Hsu, Z. G. Chi, F. B. Dias and M. R. Bryce, *Angew. Chem., Int. Ed.*, 2018, **57**, 16407–16411.
15 M. Numata, T. Yasuda and C. Adachi, *Chem. Commun.*, 2015, **51**, 9443–9446.
16 K. Shizu, H. Tanaka, M. Uejima, T. Sato, K. Tanaka, H. Kaji and C. Adachi, *J. Phys. Chem. C*, 2015, **119**, 1291–1297.
17 Q. Xue and G. H. Xie, *Adv. Opt. Mater.*, 2021, **9**, 2002204.
18 Y. Yamaguchi, Y. Matsubara, T. Ochi, T. Wakamiya and Z.-i. Yoshida, *J. Am. Chem. Soc.*, 2008, **130**, 13867–13869.
19 B.-K. An, J. Gierschner and S. Y. Park, *Acc. Chem. Res.*, 2012, **45**, 544–554.
20 J. Z. Zhao, W. H. Wu, J. F. Sun and S. Guo, *Chem. Soc. Rev.*, 2013, **42**, 5323–5351.
21 S. J. Liu, H. K. Zhang, Y. Y. Li, J. K. Liu, L. L. Du, M. Chen, R. T. K. Kwok, J. W. Y. Lam, D. L. Phillips and B. Z. Tang, *Angew. Chem., Int. Ed.*, 2018, **57**, 15189–15193.
22 Y. J. Luo, Z. G. Pang, C. Li, K. Chen, X. J. Zheng, Y. Huang and Z. Y. Lu, *J. Mater. Chem. C*, 2020, **8**, 11603–11609.
23 S. Y. Shao and L. X. Wang, *Aggregate*, 2020, **1**, 45–56.
24 M. K. Etherington, N. A. Kukhta, H. F. Higginbotham, A. Danos, A. N. Bismillah, D. R. Graves, P. R. McGonigal, N. Haase, A. Morherr, A. S. Batsanov, C. Pflumm, V. Bhalla, M. R. Bryce and A. P. Monkman, *J. Phys. Chem. C*, 2019, **123**, 11109–11117.
25 L. Salah, M. K. Etherington, A. Shuaib, A. Danos, A. A. Nazeer, B. Ghazal, A. Prlj, A. T. Turley, A. Mallick, P. R. McGonigal, B. F. E. Curchod, A. P. Monkman and S. Makhseed, *J. Mater. Chem. C*, 2021, **9**, 189–198.
26 H. Tsujimoto, D.-G. Ha, G. Markopoulos, H. S. Chae, M. A. Baldo and T. M. Swager, *J. Am. Chem. Soc.*, 2017, **139**, 4894–4900.
27 B. Li, Z. Yang, W. Q. Gong, X. H. Chen, D. W. Bruce, S. Y. Wang, H. L. Ma, Y. Liu, W. G. Zhu, Z. G. Chi and Y. F. Wang, *Adv. Opt. Mater.*, 2021, **9**, 2100180.
28 B. Z. He, J. Zhang, J. Y. Zhang, H. K. Zhang, X. Y. Wu, X. Chen, K. H. S. Kei, A. J. Qin, H. H. Y. Sung, J. W. Y. Lam and B. Z. Tang, *Adv. Sci.*, 2021, **8**, 2004299.
29 H. K. Zhang, X. Y. Zheng, N. Xie, Z. K. He, J. K. Liu, N. L. C. Leung, Y. L. Niu, X. H. Huang, K. S. Wong, R. T. K. Kwok, H. H. Y. Sung, I. D. Williams, A. J. Qin, J. W. Y. Lam and B. Z. Tang, *J. Am. Chem. Soc.*, 2017, **139**, 16264–16272.
30 J. Y. Zhang, L. R. Hu, K. H. Zhang, J. K. Liu, X. G. Li, H. R. Wang, Z. Y. Wang, H. H. Y. Sung, I. D. Williams, Z. B. Zeng, J. W. Y. Lam and H. K. Zhang, *J. Am. Chem. Soc.*, 2021, **143**, 9565–9574.
31 S. Kumar, L. G. Franca, K. Stavrou, E. Crovini, D. B. Cordes, A. M. Z. Slawin, A. P. Monkman and E. Z-Colman, *J. Phys. Chem. Lett.*, 2021, **12**, 2820–2830.
32 J. Sturala, M. K. Etherington, A. N. Bismillah, H. F. Higginbotham, W. Trewby, J. A. Aguilar, E. H. C. Bromley, A.-J. Avestro, A. P. Monkman and P. R. McGonigal, *J. Am. Chem. Soc.*, 2017, **139**, 17882–17889.
33 Z. J. Zhao, S. M. Chen, J. W. Y. Lam, Z. M. Wang, P. Lu, F. Mahtab, H. H. Y. Sung, I. D. Williams, Y. G. Ma, H. S. Kwok and B. Z. Tang, *J. Mater. Chem.*, 2011, **21**, 7210–7216.
34 S. Y. Shao, J. Hu, X. D. Wang, L. X. Wang, X. B. Jing and F. Wang, *J. Am. Chem. Soc.*, 2017, **139**, 17739–17742.
35 G. L. Niu, X. L. Zheng, Z. Zhao, H. K. Zhang, J. G. Wang, X. W. He, Y. C. Chen, X. J. Shi, C. Ma, R. T. K. Kwok, J. W. Y. Lam, H. H. Y. Sung, I. D. Williams, K. S. Wong, P. F. Wang and B. Z. Tang, *J. Am. Chem. Soc.*, 2019, **141**, 15111–15120.
36 G. P. Bartholomew and G. C. Bazan, *J. Am. Chem. Soc.*, 2002, **124**, 5183–5196.
37 H. J. Kim, P. C. Nandajan, J. Gierschner and S. Y. Park, *Adv. Funct. Mater.*, 2018, **28**, 1705141.
38 S. Lee, C.-H. Chen and A. H. Flood, *Nat. Chem.*, 2013, **5**, 704–710.
39 C. D. Fiandra, M. Moccia, V. Cerulli and M. F. Adamo, *Chem. Commun.*, 2016, **52**, 1697–1700.
40 G. B. Payne and P. H. Williams, *J. Org. Chem.*, 1961, **26**, 651–659.
41 M. Miyashita, T. Suzuki and A. Yoshikoshi, *Chem. Lett.*, 1987, 285–287.
42 S. Sugiyama, S. ÔHigashi, R. Sawa and H. Hayashi, *Bull. Chem. Soc. Jpn.*, 1989, **62**, 3202–3206.
43 H. Bouas-Laurent, A. Castellan, J.-P. Desvergne and R. Lapouyade, *Chem. Soc. Rev.*, 2000, **29**, 43–55.
44 A. Pross, L. Radom and N. V. Riggs, *J. Am. Chem. Soc.*, 1980, **102**, 2253–2259.
45 I. V. Alabugin, K. M. Gilmore and P. W. Peterson, *Wiley Interdiscip. Rev. Comput. Mol. Sci.*, 2011, **1**, 109–141.
46 T. Seko, K. Ogura, Y. Kawakami, H. Sugino, H. Toyotama and J. Tanaka, *Chem. Phys. Lett.*, 1998, **291**, 438–444.
47 D. S. Karpovich and G. J. Blanchard, *J. Phys. Chem.*, 1995, **99**, 3951–3958.
48 D. Oelkrug, A. Tompert, J. Gierschner, H.-J. Egelhaaf, M. Hanack, M. Hohloch and E. Steinhuber, *J. Phys. Chem. B*, 1998, **102**, 1902–1907.